Available online at www.sciencedirect.com
SCIENCE DIRECT
Thermochimica Acta 446 (2006) 55–65
thermochimica acta
www.elsevier.com/locate/tca

Verifying the symmetry of differential scanning calorimeters concerning heating and cooling using liquid crystal secondary temperature standards

Steffen Neuenfeld [a], Christoph Schick [b,*]

[a] *Merck KGaA, Zentrale Verfahrensentwicklung – Sicherheitstechnik, Frankfurter Str. 250, D-64271 Darmstadt, Germany*
[b] *University of Rostock, Institute of Physics, Universitätsplatz 3, D-18051 Rostock, Germany*

Available online 19 May 2006

Dedicated to Professor Wolfgang Hemminger on the occasion of his 65th anniversary.

Abstract

The German Society for Thermal Analysis (Gesellschaft für Thermische Analyse e.V.—GEFTA) recommends verifying the symmetry of differential scanning calorimeters (DSC) between heating and cooling. For this purpose the use of liquid crystal phase transitions is suggested. Merck KGaA, Darmstadt, Germany, offers three certified secondary standards for DSC calibration in heating and cooling mode, which are recommended by ASTM too. In this paper all liquid crystal phase transitions of the three liquid crystals offered are measured using different DSC's in order to verify their applicability for checking the symmetry of the instruments and the suitability for a temperature calibration in heating and cooling mode. The materials under study are: 4-cyano-4′-octylbiphenyl (8OCB, M-24 (Merck)), 4-(4-pentyl-cyclohexyl)-benzoic acid-4-propyl-phenyl ester (HP-53 (Merck)) and 4′-ethyl-4-(4-propyl-cyclohexyl)-biphenyl (BCH-52 (Merck)). The smecticA to nematic transition of M-24 (8OCB) fulfils the requirements for these purposes best. There is no detectable discontinuity in the rate dependence of the transition temperature at zero rates and the material is sufficiently stable to allow several measurements. Because of the weakness of the transition and the neighborhoods of the much stronger crystal to smecticA transition and nematic to isotropic transition instruments with sophisticated control and data treatment algorithms partly fail to detect the rate dependence of the transition correctly. In such cases HP-53 or BCH-52 can be used alternatively. In view of a temperature calibration at different temperatures in heating and cooling mode the recommended liquid crystal phase transitions are suitable. The observed supercooling effects are nearly zero for M-24 and HP-53 and less than 0.25 K for BCH-52. The liquid crystal transitions of the standards are applicable for a calibration in heating mode too.

Keywords: Temperature calibration; Liquid crystal; Differential scanning calorimeter (DSC)

1. Introduction

Temperature, heat and heat flow rate calibration of differential scanning calorimeters (DSC) is widely discussed since long. A metrologically based procedure for the temperature, heat and heat flow rate calibration of DSC was recommended by the working group 'Calibration of scanning calorimeters' of the German Society for Thermal Analysis (Gesellschaft für Thermische Analyse e.V.—GEFTA) [1–5]. Meanwhile it is recommended by ICTAC too. In the last part of the series [5] beside others the use of liquid crystal phase transitions for temperature calibration on cooling was suggested. The transitions recommended are the smecticA to nematic of 4-cyano-4′-octylbiphenyl (8OCB, M-24 (Merck)), the smecticA to nematic of 4-(4-pentyl-cyclohexyl)-benzoic acid-4-propyl-phenyl ester (HP-53 (Merck)) and the nematic to isotropic of 4′-ethyl-4-(4-propyl-cyclohexyl)-biphenyl (BCH-52 (Merck)). For all transitions it is recommended to consider the peak temperature as the transition temperature.

Although the GEFTA recommendations [1–5] are widely accepted temperature calibration of differential scanning calorimeters using secondary standards is still under discussion as can be seen from the contributions to this special issue [6–11]. Temperature calibration under extreme conditions like low temperature [7], high pressure [8,11], or fast scanning [9] are not always possible with the common metal reference materials. Especially at high rates supercooling as well as superheating of

* Corresponding author. Tel.: +49 381 498 6880; fax: +49 381 498 6882.
E-mail addresses: steffen.neuenfeld@merck.de (S. Neuenfeld), christoph.schick@uni-rostock.de (C. Schick).

0040-6031/$ – see front matter © 2006 Elsevier B.V. All rights reserved.
doi:10.1016/j.tca.2006.05.005

the transitions used for temperature calibration must be avoided. Liquid crystal transitions are therefore under discussion for DSC calibration on cooling for a long time [5,10,12–18]. Some of them are second-order transitions and should be particularly useful for calibration on cooling because significant supercooling should not appear.

In this paper the transitions of the three liquid crystals recommended in [5] were studied using different DSC apparatuses in scanning mode. In [5] supercooling is given only for the smecticA to nematic transition of 8OCB (M-24) as < 0.5 K. For the smecticA to nematic transition of HP-53 and the nematic to isotropic transition of BCH-52 supercooling is not reported in [5]. Therefore we would like to answer the questions how the rate dependence of the peak temperatures can be described and what the magnitude of supercooling for the different transitions is. For comparison we consider all liquid crystal phase transitions of the recommended compounds. Consequently the study focuses on low scanning rates on heating and cooling in order to measure the supercooling at close to equilibrium conditions and to minimize falsification due to the heat transfer in the DSC apparatuses.

2. Experimental

The liquid crystals used were 4-cyano-4′-octylbiphenyl (8OCB, M-24 (Merck)), 4-(4-pentyl-cyclohexyl)-benzoic acid-4-propyl-phenyl ester (HP-53 (Merck)) and 4′-ethyl-4-(4-propyl-cyclohexyl)-biphenyl (BCH-52 (Merck)). The certified secondary standards were provided by Merck KGaA, Darmstadt, Germany, and used without further purification. The synthesis and phase behavior is described elsewhere: M-24 [19–21], BCH-52 [22,23], HP-53 [24,25]. The indium and zinc samples were certified standards obtained from PTB Braunschweig if not otherwise stated.

The instruments applied were the Calvet type DSC 121, Setaram, France, the heat flow type DSC's Q1000, DSC 2920, TA Instruments, USA, DSC 822, Mettler-Toledo, Switzerland, and power compensation type DSC's Pyris 1 DSC and Pyris Diamond DSC, Perkin-Elmer, USA, all equipped with mechanical refrigerators as cooling device. Nitrogen was used as purge gas. The instruments were calibrated at zero heating rate according the GEFTA recommendation [4] using indium and zinc as standards. The calibrations were performed in the simplest possible way not taking into account any rate dependence if possible. Samples of different mass were prepared in standard pans as common for the different instruments. Sample mass ranges from 0.6 mg (Pyris Diamond DSC) up to 130 mg (DSC 121). The Q1000 measurements are carried out in the so-called T1 and T4P modes.

The T1 mode corresponds to a classical heat flow type DSC with a temperature and enthalpy calibrated cell. Additional calibrations were carried out in the T4P mode for corrections of imbalances, equipment heat capacities and time constants of sample and reference sensors. The calibration procedure is described in [26].

The samples were measured by cooling and heating them at varying rates through the transition under investigation. Measurements were repeated for several samples and instruments. The peak temperatures were determined from the heat flow rate curves as measured. In order to detect changes in the peak shape, typical for first order transitions, excess heat capacity was determined for the scans at different rates in heating and cooling applying the instrument's software.

3. Results

3.1. Indium

First, for comparison, an indium sample was measured. Indium shows a typical first-order melting transition which is commonly used for calibration purposes on heating; see e.g. [1,2]. In Fig. 1, the excess heat capacity measured at different heating and cooling rates for one sample is shown. The extrapolated peak onset temperature [1], which has to be used for temperature calibration in the case of first-order transitions, depends much less on rate as the peak temperature. The peak in the excess heat capacity becomes significantly sharper with decreasing rate as expected for a first-order transition. In the limit of zero rates one expects a delta function for an ideal first-order transition.

To allow a direct comparison of changes in curve shape with rate, between heating and cooling, and between the different transitions in all following plots of this kind the temperature axis spans over 7 K and the heat capacity axis for heating and cooling are the same in one plot. In order to quantify the changes in curve shape with rate the ratios between peak heights at 1 and 10 K/min were determined for heating and cooling. For indium it yields 3.7 and 8.4 for heating and cooling, respectively. The large value at cooling is due to the supercooling of about 2 K.

The extrapolated peak onset temperature and the peak temperature are plotted as a function of rate in Fig. 2. On heating the slope of the curves depends on instrument's properties and the actual thermal resistance between sample holder and sam-

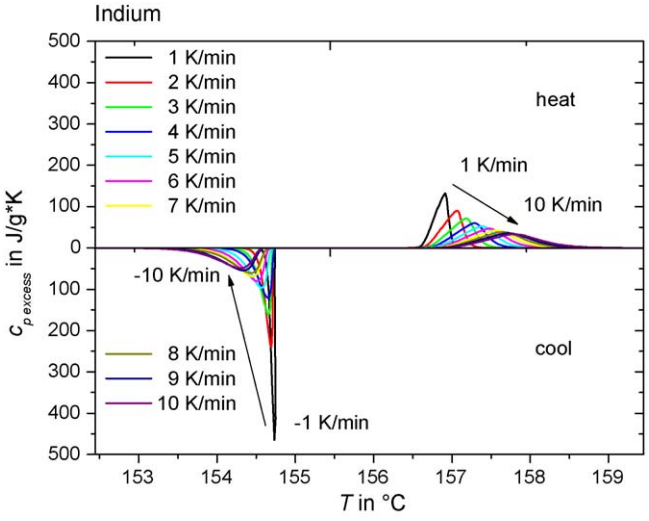

Fig. 1. Apparent specific excess heat capacities at melting and crystallization of a 2.55 mg indium sample ($\Delta H_m \approx 28.62$ J/g); Pyris 1 DSC at different rates as indicated. For the sake of clarity curves on cooling are plotted downwards.

Table 1
Parameters describing the rate dependencies of the peak (onset for In) position of the different transitions and the different instruments

Sample; instrument	τ_{lag} (min)	R (K)/60 W	*Fictive Super-cooling* (K) (from linear fits to the data at high rates)
Indium; extrapolated peak onset			
Setaram DSC 121	0.56	0	−0.75, −0.97
PE Pyris 1 DSC	0.05	0	−1.81
Mettler DSC 822	0.05	0	−1.37
TAI Q1000 T1; 2 mg	0.03	0	−1.5
TAI Q1000 T1; 11 mg	0.01	0	−0.8
TAI Q1000 T4P; 2 mg	0.007	0	−1.5
TAI Q1000 T4P; 11 mg	0.001	0	−1
Indium; peak maximum			
Setaram DSC 121	0.56	0.4	
PE Pyris 1 DSC	0.023	0.717	
Mettler DSC 822	0.067	0.503	
TAI Q1000 T1; 2 mg	0.021	0.258	
TAI Q1000 T1; 11 mg	0.025	0.079	
TAI Q1000 T4P; 2 mg	0.053	0.015	
TAI Q1000 T4P; 11 mg	0.005	0.008	
BCH-52 SmB–N			
PE Pyris 1 DSC	0.044	0.396	−0.75
Mettler DSC 822	0.065	0.254	−0.75
TAI Q1000 T1	0.094	0.508	−0.56
TAI Q1000 T4P	−0.015	0.139	−0.33
BCH-52 N–I			
PE Pyris 1 DSC	0.055	0.12	−0.18
Mettler DSC 822	0.091	0.009	−0.18
TAI Q1000 T1	0.055	0.574	−0.19
TAI Q1000 T4P	0.006	0.022	−0.04
HP-53 SmB–SmA			
PE Pyris 1 DSC	0.022	0.357	–
Mettler DSC 822	0	2.36	–
TAI Q1000 T1	0.016	0.873	–
TAI Q1000 T4P	−0.01	0.262	–
TAI DSC 2920	0.102	1.04	–
HP-53 SmA–N			
Setaram DSC 121	0.68	0	<0.05
PE Pyris 1 DSC	0.102	0.017	<0.05
Mettler DSC 822	0.04	0.5	<0.1
TAI Q1000 T1	0.037	1	−0.2
TAI Q1000 T4P	0.009	0.016	>0.01
TAI DSC 2920	0.153	0.02	−0.06
HP-53 N–I			
PE Pyris 1 DSC	0.041	0.064	−0.09
Mettler DSC 822	0.04	0.065	−0.01
TAI Q1000 T1	0.038	0.266	−0.2
TAI Q1000 T4P	0.006	0.029	−0.06
TAI DSC 2920	0.117	0.513	−0.24
M-24 SmA–N			
Setaram DSC 121	0.85	0	<0.01
PE Pyris 1 DSC	0.055	0	<0.02
Mettler DSC 822	0.075	0	<0.1
TAI Q1000 T1 (Merck)	−0.01	57	ca. 1
TAI Q1000 T4P (Merck)	0.023	6.25	−0.16
TAI Q1000 T1 (Ulm)	−0.046	247	ca. −1.6
TAI Q1000 T4P (Ulm)	0.022	28	−0.5

Table 1 (*Continued*)

Sample; instrument	τ_{lag} (min)	R (K)/60 W	*Fictive Super-cooling* (K) (from linear fits to the data at high rates)
M-24 N–I			
Setaram DSC 121	0.723	0.068	−0.22
PE Pyris 1 DSC	0.11	0.359	−0.2
Mettler DSC 822	0.134	0.082	−0.22
TAI Q1000 T1	0.035	0.188	−0.14
TAI Q1000 T4P	0.004	0.062	−0.07

R and τ_{lag} were obtained by least square fitting of Eq. (2) to the data, see text.

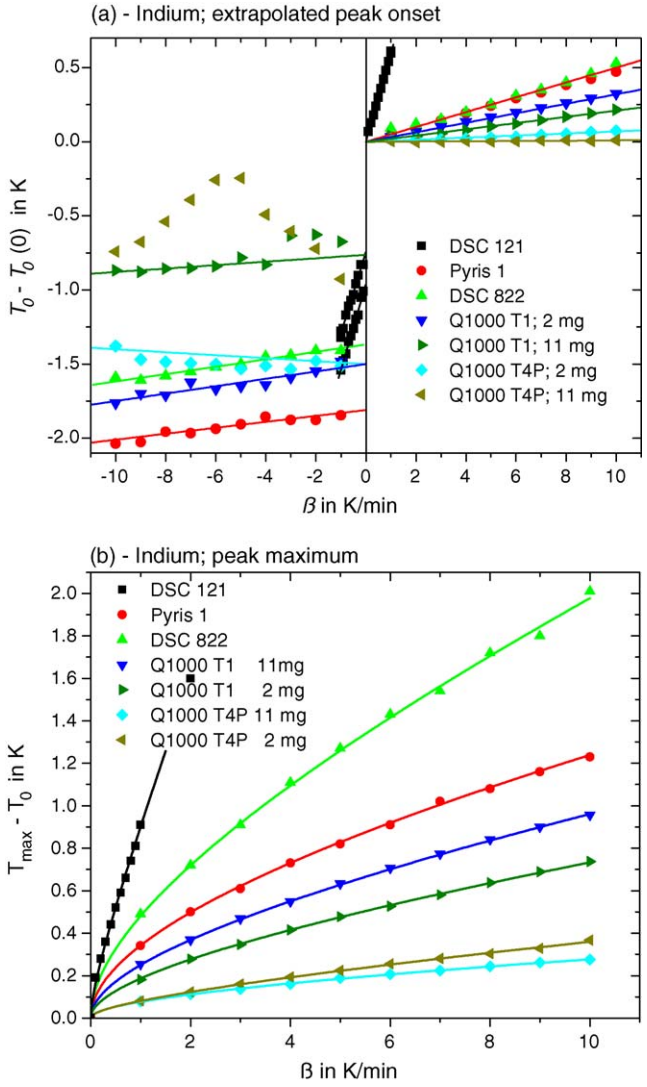

Fig. 2. (a) Extrapolated peak onset temperatures, T_0, for melting and crystallization of indium, $T_0(0) = 156.6\,^{\circ}C$ (heating rate = 0). (b) Shift of the peak maximum temperatures for melting. Sample masses: DSC 121 – 5 mg, Pyris 1 DSC – 2.5 mg, DSC 822 – 6 mg, Q1000 1.86 mg and 11.11 mg. All curves are fitted by the rate dependence according to Illers [27], see text. The fit parameters are given in Table 1.

ple, which may change from sample to sample. Therefore the extrapolation to zero heating rates is obligatory for a precise determination of a transition temperature from DSC measurements as described in the GEFTA recommendation [1,2]. A second obvious feature in the curves is the discontinuity at zero rate due to the supercooling of about 2 K, see Table 1. Supercooling is not well reproducible as seen from the scatter in the data on cooling. Consequently indium and other pure metals cannot easily be used for DSC calibration on cooling [5].

The slope for the cooling part of the extrapolated peak onset dependency in Fig. 2a is about half of that of the heating part. T_0 at cooling is not only determined by instrumental lags as for heating but supercooling depends on other factors too. For these experiments different indium samples were used (PTB reference material, TA Instruments calibration kit from 2003, Perkin-Elmer calibration kit from 1976) and measured in different pans. Different values for the supercooling are observed. For the DSC 121 the sample consists of two pieces of indium and two independent crystallization peaks indicating different supercoolings can be seen simultaneously in one cooling run. In the heating curves always a single melting peak is observed as expected for pure metals. The data points for cooling in T4P mode of the Q1000 do not follow a linear trend. Even at higher cooling rate super cooling becomes smaller resulting in a negative slope of the linear fit curve. This effect becomes more pronounced for larger sample masses. The reason for that unphysical behavior is not yet known.

The peak maximum is additionally shifted because of the latent heat to be transferred into the sample, which stays at constant temperature during the transition at heating. This effect and the consequences for DSC measurements were discussed in detail by Illers [27] and in this issue by Poel and Mathot [9]. For the shift of the maximum with rate Eq. (1) was derived for not too high heating rates and sample masses:

$$T_{\max} - T_0 = \sqrt{2\Delta H_m R\beta} + \tau_{\text{lag}}\beta \quad (1)$$

with T_0 is the "true" melting temperature for an ideal first-order phase transition; ΔH_m the enthalpy change at the transition; R the effective thermal resistance; τ_{lag} the time constant due to thermal lag, depending on heat capacity and thermal resistance; β the heating rate. The curves in Fig. 2 are fits of Eq. (1) to the rate dependencies. The fit parameters are given in Table 1. Due to the construction employed for the determination of the extrapolated peak onset temperature, Fig. 2a, the square root term in Eq. (1) does not contribute to the observed shift. Only the thermal lag described by the second term, which depends on the instrument and the software settings, contributes to the shift. For indium Eq. (1) describes the observed shifts very well, as expected.

To avoid supercooling second-order phase transitions with as small as possible rearrangement of the structure during the transition should be used instead of first-order transitions. Several liquid crystal phase changes are second or weak first-order phase transitions and thus eventually useful for temperature calibration on cooling. Next, the liquid crystals recommended in [5], which are offered by Merck KGaA, Darmstadt [28] as certified secondary reference materials for DSC temperature calibration, were checked.

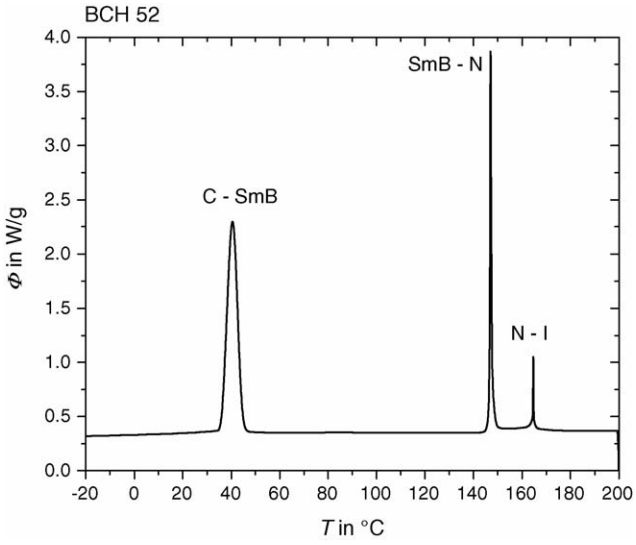

Fig. 3. Transitions of BCH-52 at heating a 3.47 mg sample in a standard pan at 10 K/min, TAI Q1000 DSC in T4P mode.

3.2. BCH-52

Fig. 3 shows the phase transitions in the liquid crystal BCH-52.

The crystalline to smecticB transition (C–SmB) is of first-order and not considered further. Excess heat capacity for the smecticB to nematic (SmB–N) and the nematic to isotropic (N–I) transitions at different rates are presented in Fig. 4.

For second-order phase transitions and without smearing by the instrument the curves should be independent on rate. But the curves at lower rates show sharper peaks. It is not easy to distinguish if the smearing is only due to the instrument or if the transition is not of second order. Obviously there is not such strong supercooling as for indium, see Fig. 1. The ratio for the peak heights at 1 and 10 K/min yields for the smecticB to nematic transition 3.2 and 3.4 for heating and cooling, respectively, and for the nematic to isotropic transition 4.7 and 5.2, respectively. The value of 4.7 on heating through the nematic to isotropic transition is even larger as the corresponding value for indium. This indicates some additional smearing inside the sample not expected for indium where the sample temperature is kept constant during melting because of the high thermal conductivity of the metal. Because there is some smearing the peak position will not only depend on thermal lag due to heat capacity and an effective thermal resistance. To take into account the larger amount of heat transferred into the sample in the transition range we applied Eq. (1) to the measured peak temperature as shown in Fig. 5. Eq. (1) was derived for a first-order phase transition, which is certainly not present here. But from Figs. 4 and 5 it becomes obvious that there is an additional contribution to the observed shift related to the changes in peak shape. For formal reasons we apply Eq. (1) knowing about the limitations of this approach for true or partial second-order transitions. Assum-

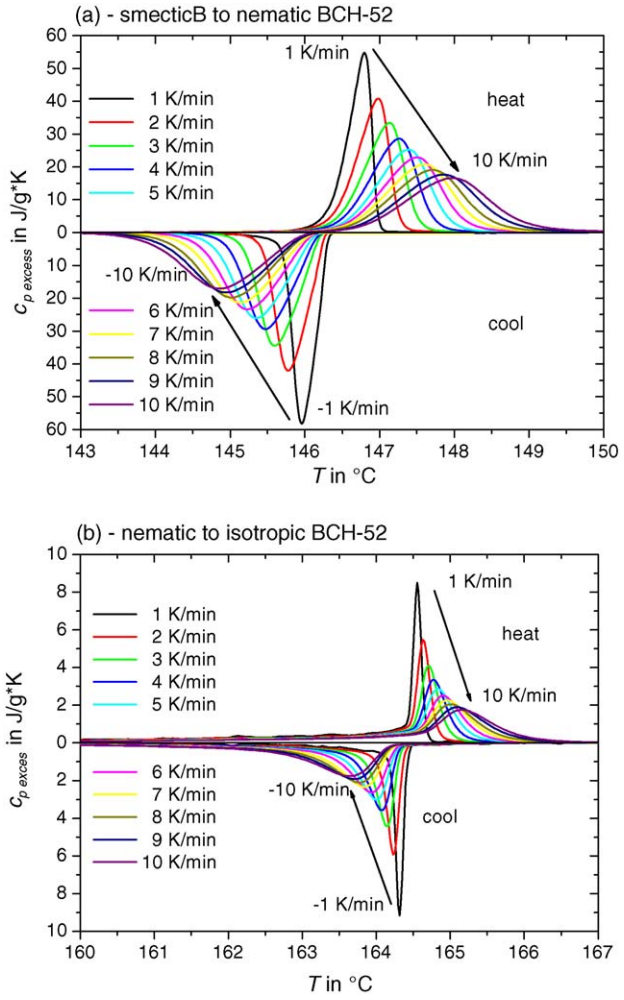

Fig. 4. Specific apparent excess heat capacities of BCH-52 in (a) the smecticB to nematic ($\Delta H \approx 24$ J/g) and (b) the nematic to isotropic ($\Delta H \approx 2.5$ J/g) (recommended in [5]) transition range at different rates. For the sake of clarity curves on cooling are plotted downwards. Pyris Diamond DSC, 6.7 mg.

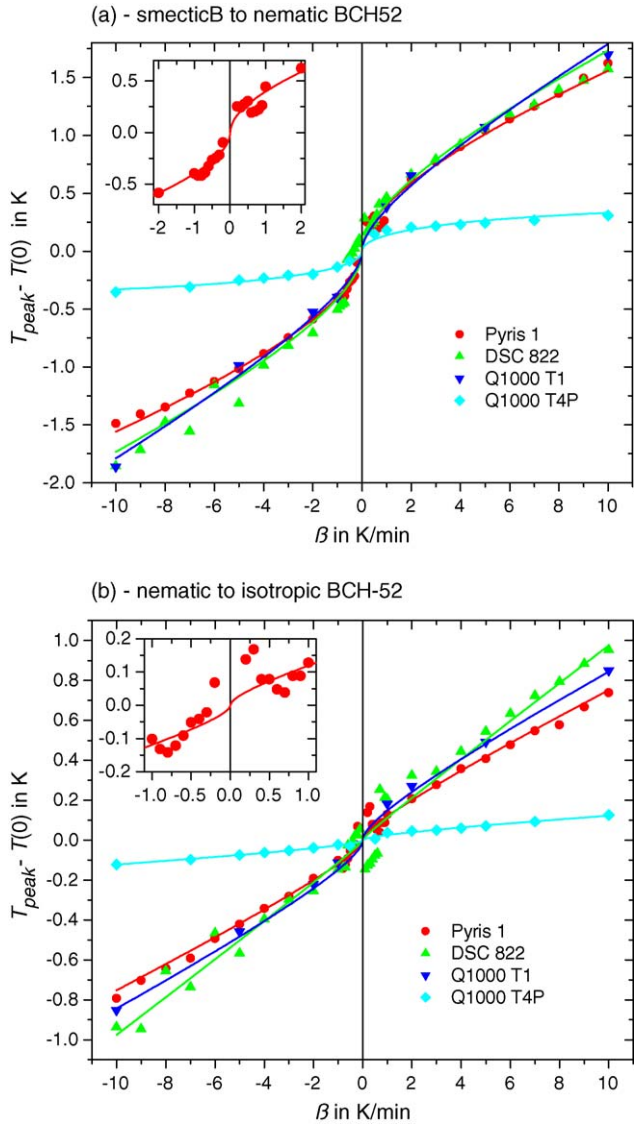

Fig. 5. Rate dependence of the peak temperature for (a) smecticB to nematic, $T_0 = 146.8 \pm 0.4$ °C, and (b) the nematic to isotropic, $T_0 = 164.8 \pm 0.4$ °C, transition (recommended in [5]) of BCH-52. Sample masses: Pyris 1 DSC – 6.7 mg, DSC 822 – 9.8 mg, Q1000 T1 – 3 mg, Q1000 T4P 3.5 mg. The inset shows the region around zero rates for the Pyris 1 DSC. Curves are fits of Eq. (2) to the data. The fit parameters are given in Table 1.

ing some symmetry between heating and cooling of the studied transitions we modified Eq. (1) in order to allow simultaneous fitting of the heating and cooling parts of the rate dependencies. Actually the following equation was used for fitting the maxima of the liquid crystal phase transitions:

$$T_{\max} - T_0 = \frac{\beta}{\mathrm{abs}(\beta)}\sqrt{2\Delta H R\,\mathrm{abs}(\beta)} + \tau_{\mathrm{lag}}\beta \qquad (2)$$

With ΔH the enthalpy changes in the transition range and β heating (+) or cooling (−) rate. Some of the liquid crystal transitions are lambda shaped and very broad. Particular for these transitions the prerequisites of the model are not fulfilled. Additionally the determination of the enthalpy change, which is the cause for the smearing of the peaks, becomes difficult [21]. The values used are given in the figure captions of Figs. 1, 4, 7 and 11. Finally R and τ_{lag} were determined by a non-linear least squares fit procedure. The results are given in Table 1.

For both mesomorphic transitions in BCH-52 the rate dependence is well described by Eq. (2). The parameters are given in Table 1. The contribution of the square root term is smaller for the nematic to isotropic transition compared to the smecticB to nematic transition. The smecticB to nematic transition shows a difference between the more or less linear parts of the dependencies at higher rates of about 0.7 K and the nematic to isotropic transition of about 0.2 K. These values, presented as fictive super-cooling in Table 1, are independent on the instrument or instrument type applied except the Q1000 in T4P mode. The direct comparison between the power compensated Pyris 1 DSC, the heat flux type DSC 822 and the Q1000 in T1 mode yields nearly the same values for super-cooling even the slope of the curves differs slightly between the three instruments, see fit parameters in Table 1. The τ_{lag} values are in most cases in the same order of magnitude as for the indium measurements. Possibly due to the T4P calibration an unrealistic negative τ_{lag} value for the Q1000 in T4P mode results from an over-correction

of the instrument's heat transfer contribution. The values for the effective thermal resistance R and consequently the square root term in Eq. (2) cannot be neglected. R shows much larger scatter compared to τ_{lag} regarding the two transitions. The different values for R for the same sample in the same measurement indicate the deviation from the model of a first-order phase transition as it is assumed for Eq. (2). From Figs. 4 and 5 it can be concluded that both transitions are neither of true first order nor of true second order. Liquid crystal phase transitions are often so-called weakly first-order transition with distinct pre-transitional fluctuation effects. Both show non-linear rate dependence and apparent excess heat capacity depends strongly on rate. The rate dependencies are formally well described by Eq. (2) without any discontinuity at zero rates. For the nematic to isotropic transition a relatively large scatter of the data points at rates below 1 K/min is observed. A similar observation is reported by Sarge for the nematic to isotropic transition of 4,4′-azoxyanisole [10].

3.3. HP-53

The liquid crystal HP-53 undergoes three mesomorphic transitions as presented in Fig. 6. The compound is therefore and because of the different peak heights of particular interest for calibration purposes.

In Fig. 7, the apparent excess heat capacities for the different transitions are shown.

All three transitions do not show large supercooling. The ratio of the peak heights for 1 K/min to that for 10 K/min for heating and cooling, respectively, yields the following values: smecticB to smecticA 3.3 on heating, 3.7 on cooling; smecticA to nematic 2.8 on heating, 2.5 on cooling; nematic to isotropic 4 on heating, 4.6 on cooling. The smecticA to nematic transition is much smaller than the other two. But the transition is much broader compared to the other transitions. The nematic to isotropic transition at about 181 °C is influenced by an oxidative

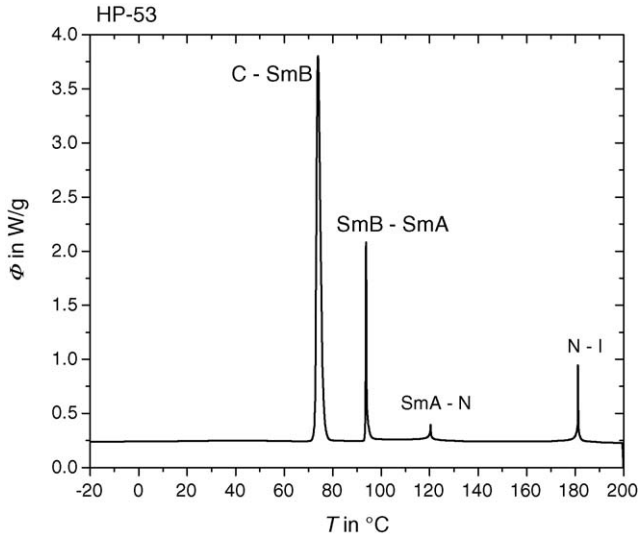

Fig. 6. Transitions of HP-53 at heating a 4 mg sample in a standard pan at 10 K/min, TAI Q1000 DSC in T4P mode.

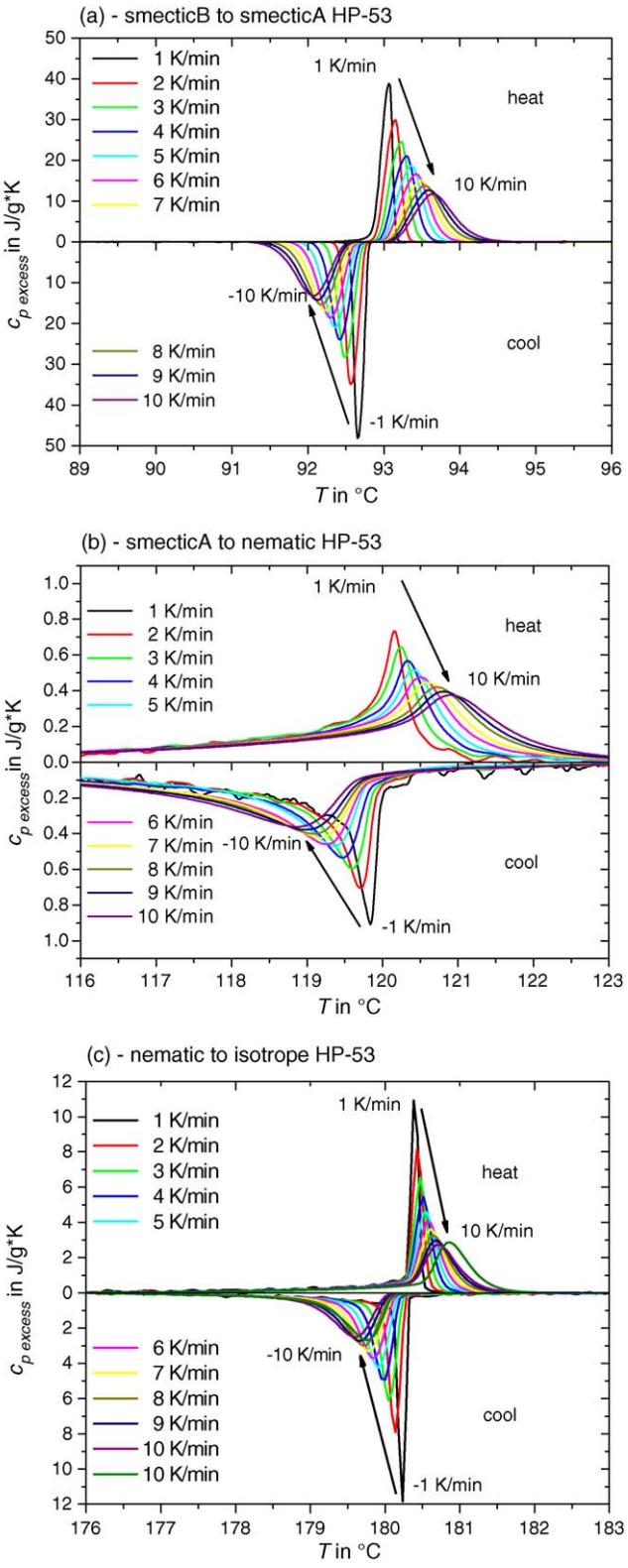

Fig. 7. Specific apparent excess heat capacities of HP-53 in (a) the smecticB to smecticA ($\Delta H_m \approx 8$ J/g), (b) the smecticA to nematic ($\Delta H_m \approx 1$ J/g) (recommended in [5]) and (c) the nematic to isotropic ($\Delta H_m \approx 3$ J/g) transition range at different rates. For the sake of clarity curves on cooling are plotted downwards. Pyris Diamond DSC, 5.5 mg.

degradation at such high temperature resulting from the oxygen residue in the pan. The two curves for 10 K/min heating rate in Fig. 7c, measured at the beginning and the end of the experiment, show a shift of a few tenth of a Kelvin. Oxygen reducing sample preparation or work with fresh samples is recommended in this case.

In Fig. 8, the rate dependence of the peak temperature is shown for the different transitions.

The dependence for the smecticB to smecticA transition (a) can again be fitted by Eq. (2). Approaching zero heating and cooling rates a strong non-linear behavior is observed. Similar curves were obtained for the lambda shaped solid–solid phase transition in NH_4Cl [13]. Here the square root term in Eq. (2) cannot be neglected. At rates below 1 K/min small deviations from the fit curve are visible, see inset in Fig. 8a. A closer inspection of the curves for the lowest rates yields some peculiarities in the curve shape, which may be related to the somehow untypical rate dependence. In Fig. 9, the heating curves below 0.1 K/min show a broad plateau at the maximum and the cooling curves exhibit a shoulder at about 93.65 °C or as for the 0.05 K/min curve again a plateau or even two maxima. The smecticB to smecticA transition of HP-53 is therefore not suitable for temperature calibration of DSC's on cooling.

For the smecticA to nematic transition of HP-53 nearly straight lines fit heating and cooling, see Fig. 8b. But the slopes of the curves for heating and cooling are slightly different. In general they are larger than for indium, see Table 1. This could indicate some thermal lag inside the sample, which is expected for organic compounds. The square root term in Eq. (2) is not very important because of the small enthalpy change and the relatively small effective thermal resistance. At low rates some additional scatter in the data is observed for all instruments. Because of the small peak it is difficult to obtain data with sufficient signal to noise ratio. Here some scatter in the temperature as shown in Fig. 9 may play a role too.

Because there is no discontinuity at zero rates and the shift of the peak due to the enthalpy change is small, except for the TAI Q1000 in T1 mode, the smecticA to nematic transition of HP-53 may be used for calibration of DSC's on cooling. Supercooling is less than 0.1 K. But the different slopes for heating and cooling introduce additional uncertainties, which could be interpreted as an asymmetry of the instrument checked.

The nematic to isotropic transition of HP-53 shows again a significant change in slope of the rate dependency at zero rates, see Fig. 8c. The slope of the curves is similar to that obtained for indium on heating. It should be mentioned that for the same sample in the same measurement different slopes are found for the different transitions. Of particular interest is the observation that the slope of the much smaller smecticA to nematic transition is for some instruments larger than that found for the much stronger nematic to isotropic transition. This cannot be explained by thermal lag inside the sample due to low thermal conductivity.

Summarizing, the nematic to isotropic transition shows some untypical behavior like the different slopes for heating and cooling and a large contribution from the square root term in Eq. (2) to the rate dependencies. This transition is therefore also not

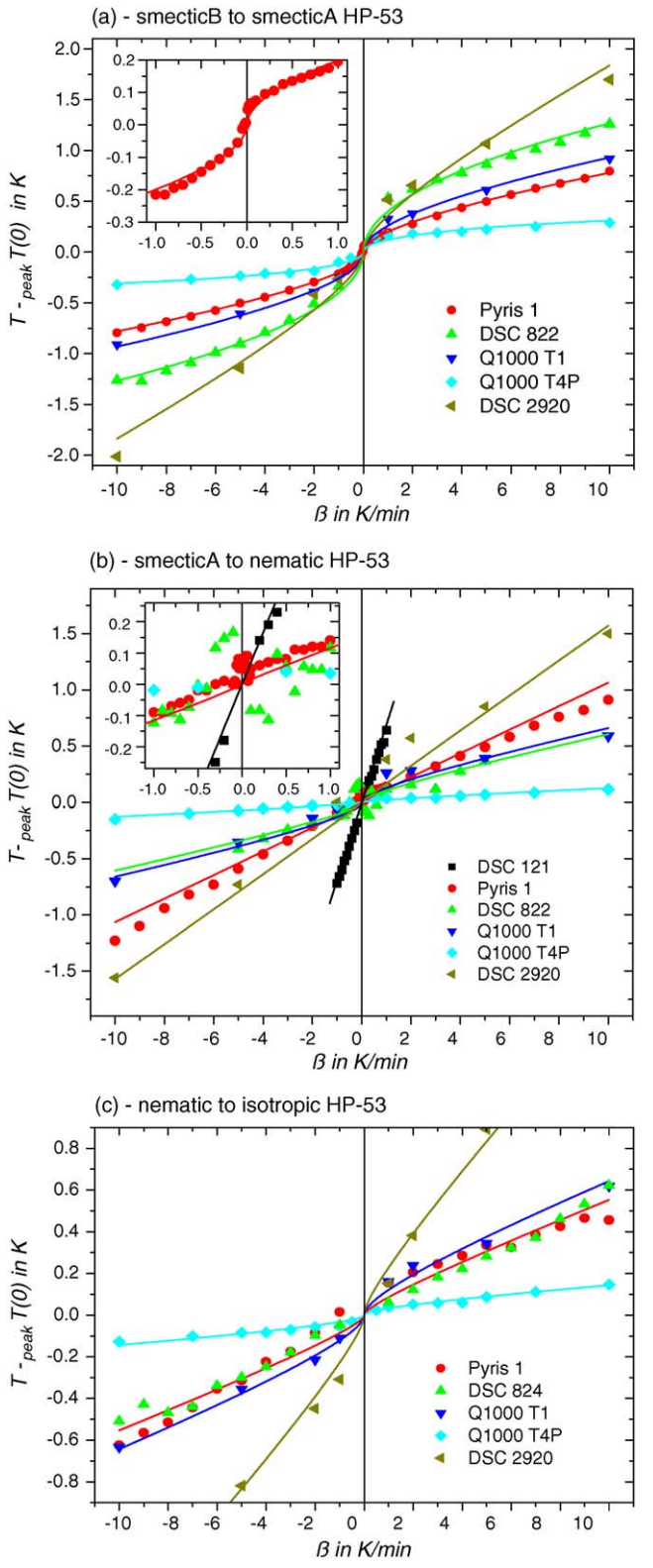

Fig. 8. Rate dependence of the peak temperature for (a) smecticB to smecticA, $T_0 = 93.7 \pm 0.4$ °C, (b) smecticA to nematic, $T_0 = 120.5 \pm 0.4$ °C (recommended in [5]), and (c) the nematic to isotropic, $T_0 = 181.2 \pm 1$ °C, transition of HP-53. Sample masses: DSC 121 – 24.2 mg, Pyris 1 DSC – 5.5 mg, DSC 822 – 4.2 mg, Q1000 T1 – 4.2 mg, Q1000 T4P – 4 mg, DSC 2920 – 3.4 mg. Curves are fits of Eq. (2) to the data. The fit parameters are given in Table 1.

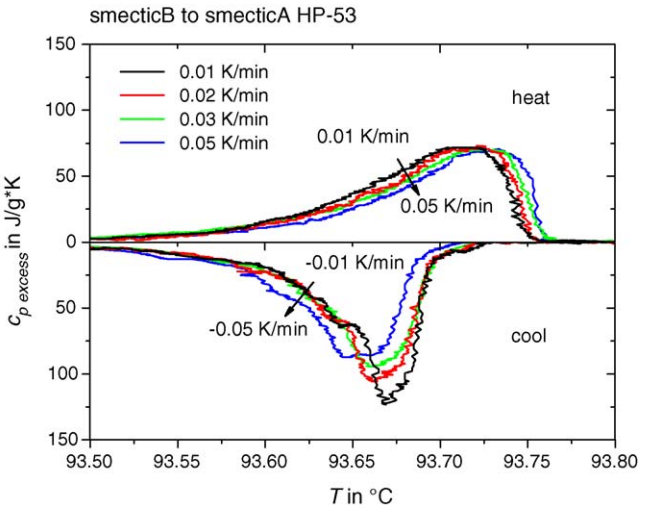

Fig. 9. Specific apparent excess heat capacities of HP-53 in the smecticB to smecticA transition range at the lowest rates. For the sake of clarity curves on cooling are plotted downwards. Pyris Diamond DSC, 5.5 mg.

suitable for calibration of DSC's on cooling or for checking the symmetry of the instrument.

3.4. M-24

The liquid crystal M-24 (8OCB) undergoes two mesomorphic transitions as presented in Fig. 10. The compound was already used for calibration of DSC's on cooling [14,15] and in temperature modulated mode (TMDSC) [29,30] and other calorimeters [31,32]. It is therefore of particular interest for calibration purposes.

Fig. 11 shows the apparent excess heat capacities for the different transitions.

Both mesomorphic transitions do not show large supercooling. The ratio of the peak heights for 1 K/min to that for 10 K/min

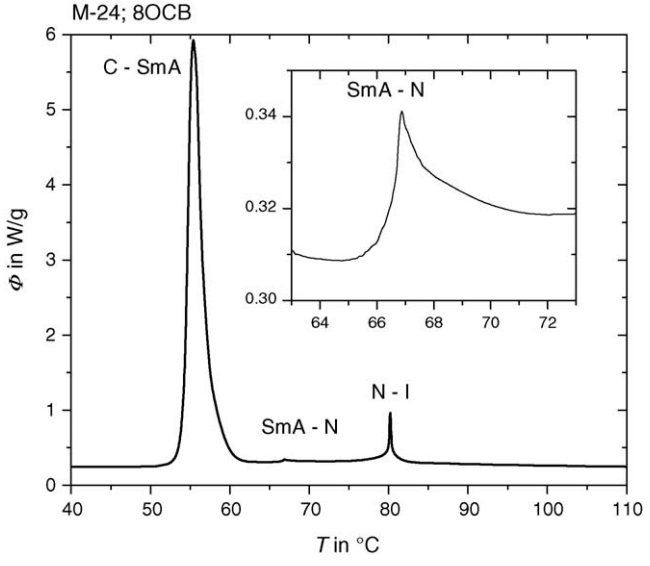

Fig. 10. Transitions of M-24 (8OCB) at heating a 5.6 mg sample in a standard pan at 10 K/min, TAI Q1000 DSC in T4P mode.

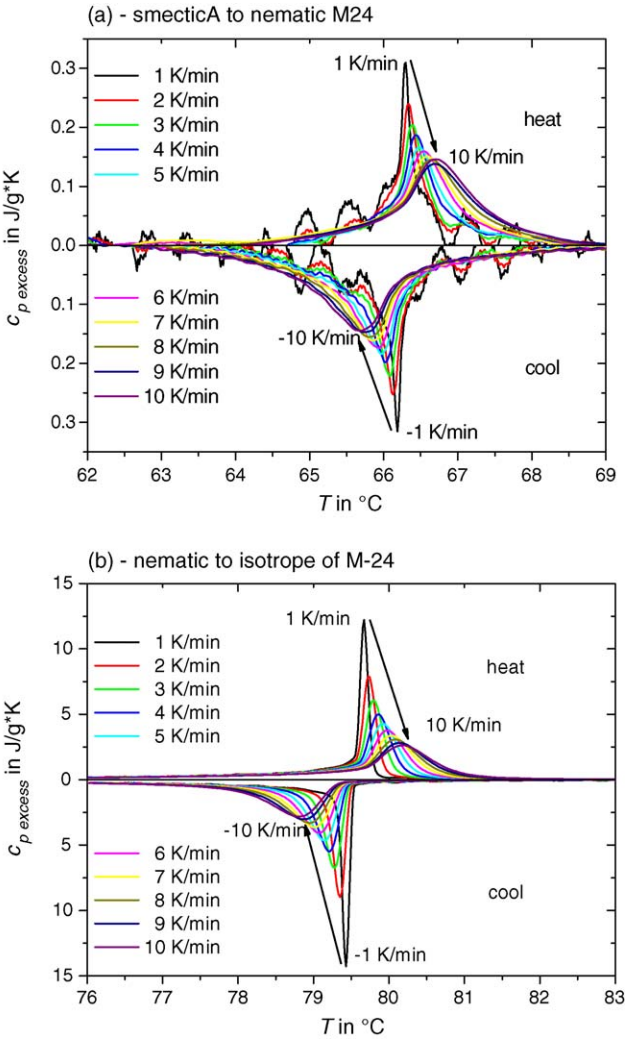

Fig. 11. Specific apparent excess heat capacities of M-24 in (a) the smecticA to nematic ($\Delta H_m \approx 0.2$ J/g) (recommended in [5]) and (b) the nematic to isotropic ($\Delta H_m \approx 3$ J/g) transition range at different rates. For the sake of clarity curves on cooling are plotted downwards. Pyris Diamond DSC, 5.1 mg.

for heating and cooling, respectively, yields the following values: smecticA to nematic 2.1 on heating, 2.2 on cooling; nematic to isotropic 4.7 on heating, 5.1 on cooling. The smecticA to nematic transition is much smaller than the nematic to isotropic transition and sometimes hard to detect because it may be influenced by the crystal to smecticA and the neamtic to isotropic transitions at high rates.

In Fig. 12, the rate dependence of the peak temperature is shown for both transitions.

The rate dependencies found for the smecticA to nematic transition does not show any supercooling except the measurements performed with two different Q1000 Dsc's in T1 as well as in T4P mode. For all other instruments one straight line simultaneously fits the points for heating and cooling. Because of the small enthalpy change for this transition the square root term in Eq. (2) cannot play an important role. The difference between the linear dependencies for heating and cooling (supercooling) is less than 0.01 K as shown in the inset for the Pyris 1 and in Fig. 13 below for the DSC 121. Similar results were

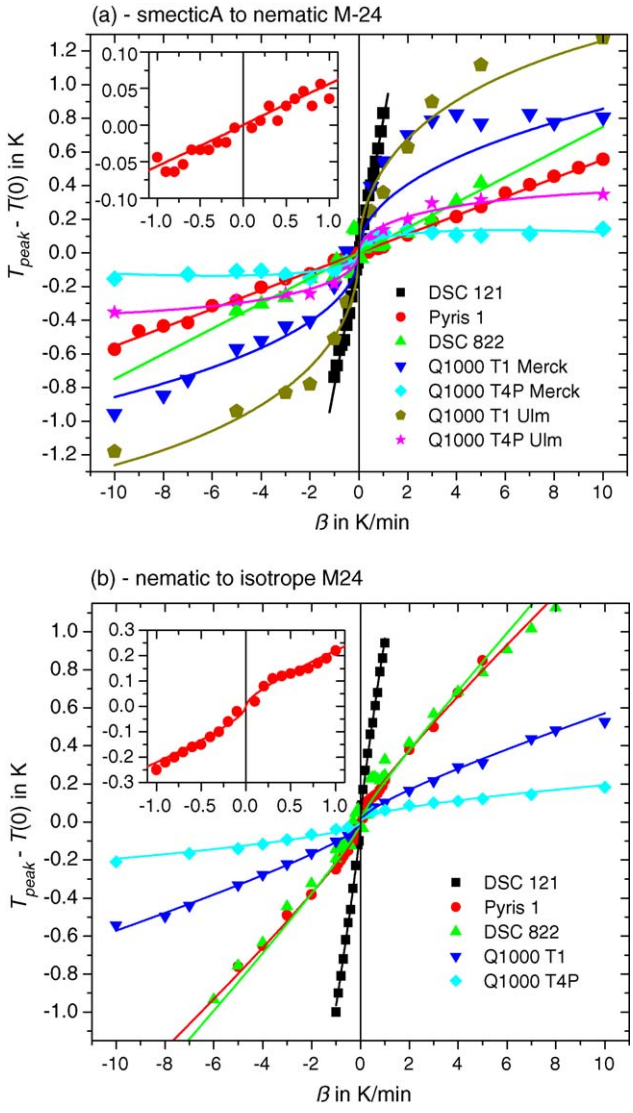

Fig. 12. Rate dependence of the peak temperature for (a) smecticA to nematic, $T_0 = 67.4 \pm 0.4\,^{\circ}C$ (recommended in [5]), and (b) the nematic to isotropic, $T_0 = 80.2 \pm 0.4\,^{\circ}C$, transition of M-24 (8OCB). Sample masses: DSC 121 – 128.9 mg, Pyris 1 DSC – 5.1 mg DSC 822 – 10.9 mg, Q1000 T1 Merck – 4 mg, Q1000 T4P Merck – 5.6 mg, Q1000 Ulm – 2.9 mg. The inset shows the region near zero rates for the Pyris 1 DSC. Curves are fits of Eq. (2) to the data. The fit parameters are given in Table 1.

already reported in [14,15]. The data from the DSC 822 exhibit some peculiarities at low rates. Below 0.5 K/min some scatter appears similar to the behavior found for the smecticA to nematic transition of HP 53, see Fig. 8. A more serious problem is detected for the Q1000. For the Q1000 in T1 modus the data show a step of more than 1 K at zero rates. In the T4P modus the step is reduced to about 0.1 K for the instrument at Merck but is about 0.5 K for the instrument in Ulm. Both discontinuities are significantly larger as measured with all other instruments.

For the nematic to isotropic transition a step of about 0.2 K is observed for all instruments except the Q1000—here the step is 0.14 K in T1 and 0.07 K in T4P mode only.

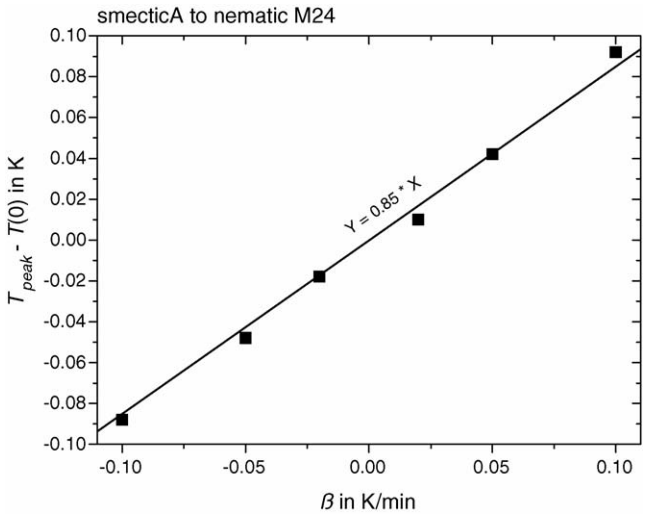

Fig. 13. Rate dependence of the peak temperature for the smecticA to nematic transition of M-24 (8OCB) at very low rates. Sample mass 129.9 mg, $T_0 = 67.4 \pm 0.4\,^{\circ}C$, DSC 121.

4. Discussion

The different phase transitions of the liquid crystals recommended in [5] show significant different rate dependencies as shown in Figs. 5, 8, 12 and 13. Because some of them are not at all suitable for temperature calibration or verification of symmetry between heating and cooling of DCS's the GEFTA working group recommended only the following transitions: the nematic to isotropic of 4′-ethyl-4-(4-propyl-cyclohexyl)-biphenyl (BCH-52 (Merck)), the smecticA to nematic of 4-(4-pentyl-cyclohexyl)-benzoic acid-4-propyl-phenyl ester (HP-53 (Merck)) and the smecticA to nematic of 4-cyano-4′-octylbiphenyl (8OCB, M-24 (Merck)). These transitions were studied in detail in order to verify their applicability for calibration purposes. All rate dependencies could be fitted by Eq. (2) based on the approach by Illers [27]. The equation was derived for first-order phase transitions. Here we use Eq. (2) assuming a similar response of the instruments to the relative sharp maxima of the liquid crystal transitions, which are assumed to be comparable to first-order transitions. The weakness of this approach can be seen from the fit parameters given in Table 1. For different transitions in the same sample different values for τ_{lag} as well as for R were found. The rate dependence of the peak maxima of the liquid crystal transitions is very complex. A sufficient description needs a more complex model to take into account the peak shape and the enthalpy change associated to the transitions. But for the transitions under investigation, which are assumed to be of weakly first order or of second order, a linear rate dependency is often not found and the smearing of the peaks must be considered in an appropriate way. The use of Eq. (2) results in a formal fitting of the dependencies, which allows us to test the applicability of the transitions for temperature calibration and for the check of symmetry between heating and cooling of DSC apparatuses.

The nematic to isotropic transition of BCH-52 shows some difference between the linear dependencies for heating and cool-

ing of about 0.2 K. If this is sufficient it can be used for symmetry checking and calibration in cooling as well as heating mode. The smecticA to nematic transition of HP-53 does not show a discontinuity in respect of a step at zero rates but it shows a change in the slope going from heating to cooling. This is not well understood and results possibly from the complex nature of the liquid crystal phase transition. This transition of HP-53 is suitable for calibration of DSC's on cooling. The different slopes for heating and cooling should be taken into consideration for checking the symmetry. For the smecticA to nematic transition of M-24 (8OCB) it was shown before [14,15,29–32] that there is a linear rate dependency and nearly no discontinuity at zero rates. Neither a step nor a change in slope was detected at zero rates. This was verified in this study again. Therefore we recommend using the smecticA to nematic transition of M-24 to verify the symmetry of DSC apparatuses in regard to heating and cooling.

The smecticA to nematic transition of M-24 is very weak. Therefore it needs high sensitive calorimeters to detect the transition. Obviously the data treatment routines of the TAI DSC Q1000 cannot handle such transitions correctly. The observed behavior for these instruments is not feasible, neither in T1 nor in T4P mode. The results presented in Fig. 12a were verified for several samples and the discontinuity near zero rates became stronger for smaller sample masses. To exclude wrong calibration as the reason for the observed behavior the measurements were repeated on another instrument at IFA GmbH in Ulm. The illogical behavior appears again. Eventually the large crystalline to smecticA or the nematic to isotropic transition at about 10 K lower or higher temperature, respectively, forces the instrument to compensate for some effects which are not present anymore at the very weak smecticA to nematic transition of M-24. Eventually the instrument (control circuits, data treatment?) has not totally recovered from that event and therefore falsifies the measurement. Similar problems were detected for indium cooling measurements, see Fig. 2. The reason for this behavior is not known so far and needs further investigations.

5. Conclusions

We recommend using the smecticA to nematic transition of 4-cyano-4′-octylbiphenyl (M-24, 8OCB) to verify the symmetry between heating and cooling of DSC's. M-24 can be used as a secondary standard for temperature calibration in heating and cooling mode and is available from Merck KGaA [28]. The smecticA to nematic transition of HP-53 or the nematic to isotropic transition of BCH-52 can be used alternatively.

A carefully check of the symmetry of the DSC apparatuses is obligatory if measurements on cooling or isothermal experiments are performed. On the example of the TAI DSC Q1000 the problem is confirmed in a drastic way. The concept of the instrument and the data treatment becomes questionable considering the results for the smecticA to nematic transition of M-24 but also for the crystallization of indium.

Acknowledgements

The authors acknowledge helpful discussions with A.A. Minakov and G.W.H. Höhne and his kindness to repeat measurements on the TAI Q1000 DSC at IFA GmbH in Ulm, Germany.

References

[1] G.W.H. Höhne, H.K. Cammenga, W. Eysel, E. Gmelin, W. Hemminger, The temperature calibration of scanning calorimeters, Thermochim. Acta 160 (1990) 1–12.
[2] H.K. Cammenga, W. Eysel, E. Gmelin, W. Hemminger, G.W.H. Höhne, S.M. Sarge, The temperature calibration of scanning calorimeters. Part 2. Calibration substances, Thermochim. Acta 219 (1993) 333–342.
[3] S.M. Sarge, E. Gmelin, G.W.H. Höhne, H.K. Cammenga, W. Hemminger, W. Eysel, The caloric calibration of scanning calorimeters, Thermochim. Acta 247 (1994) 129–168.
[4] S.M. Sarge, W. Hemminger, E. Gmelin, G.W.H. Höhne, H.K. Cammenga, W. Eysel, Metrologically based procedures for the temperature, heat and heat flow rate calibration of DSC, J. Therm. Anal. 49 (1997) 1125–1134.
[5] S.M. Sarge, G.W.H. Höhne, H.K. Cammenga, W. Eysel, E. Gmelin, Temperature, heat and heat flow rate calibration of scanning calorimeters in the cooling mode, Thermochim. Acta 361 (2000) 1–20.
[6] T. Charsley, P.G. Laye, V. Palakollu, J.J. Rooney, B. Joseph, DSC studies on organic melting point temperature standards, Thermochim. Acta 446 (2006) 29–32.
[7] P. van Ekeren, A. van Genderen, G. van den Berg, Redetermination of the thermodynamic properties of the solid–solid transition of Adamantane by adiabatic calorimetry to investigate the suitability as a reference material for low-temperature DSC-calibration, Thermochim. Acta 446 (2006) 33–35.
[8] J. Ledru, C.T. Imrie, J.M. Hutchinson, G.W.H. Höhne, High pressure differential scanning calorimetry: aspects of calibration, Thermochim. Acta 446 (2006) 66–72.
[9] G.V. Poel, V.B.F. Mathot, High speed/high performance differential scanning calorimetry (HPer DSC): temperature calibration in the heating and cooling mode and minimization of thermal lag, Thermochim. Acta 446 (2006) 41–54.
[10] H.K. Cammenga, K. Gehrich, S.M. Sarge, 4,4′-Azoxyanisole for temperature calibration of differential scanning calorimeters in the cooling mode—yes or no? Thermochim. Acta 446 (2006) 36–40.
[11] F. Dan, J.-P.E. Grolier, High pressure–low temperature calorimetry. I. Application to the phase change of mercury under pressure, Thermochim. Acta 446 (2006) 73–83.
[12] J.D. Menczel, T.M. Leslie, Temperature calibration of a power compensation DSC on cooling, Thermochim. Acta 166 (1990) 309–317.
[13] C. Schick, G.W.H. Höhne, On temperature calibration of power compensation DSC in cooling mode, Thermochim. Acta 187 (1991) 351–356.
[14] G.W.H. Höhne, J. Schawe, C. Schick, Temperature calibration on cooling using liquid crystal phase transitions, Thermochim. Acta 221 (1993) 129–137.
[15] P. Skoglund, A. Fransson, Accurate temperature calibration of differential scanning calorimeters, Thermochim. Acta 276 (1996) 27–39.
[16] G. Hakvoort, C.M. Hol, P.J. van Ekeren, DSC calibration during cooling; a survey of possible compounds, J. Therm. Anal. 64 (2001) 367–375.
[17] J.A. Martins, J.J.C. Cruz-Pinto, The temperature calibration on cooling of differential scanning calorimeters, Thermochim. Acta 332 (1999) 179–188.
[18] M.J.A. Malheiro, J.A. Martins, J.J.C. Cruz Pinto, Evaluation of the calibration errors on cooling of a differential scanning calorimeter using different sets of standard metals, Thermochim. Acta 420 (2004) 155–161.
[19] Patent: Merck DE 2450088 (1976); Chem. Abstr. EN 85 46219.
[20] G.W. Gray, J.E. Lydon, New type of smectic mesophase? Nature 252 (1974) 221–222.

[21] B.R. Ratna, S. Chandrasekhar, Some comments on the determination of enthalpies of liquid crystalline transitions by differential scanning calorimetry, Mol. Cryst. Liq. Cryst. 162B (1988) 157–159.
[22] Patent: Merck DE 2927277 (1979).
[23] R. Eidenschinck, Low viscous compounds of highly nematic character, Mol. Cryst. Liq. Cryst. 94 (1983) 119–125.
[24] Patent: Merck DE 2800553 (1979). Chem. Abstr. EN 91 140584.
[25] K. Bhowmick, A. Mukhopadhyay, S.K. Roy, The temperature dependence of the orientational order parameter of the mesogens: 4′-*n*-propyl phenyl-4-(4′-*n*-pentyl cyclohexyl) benzoate, trans-4-propyl cyclohexyl 4-(trans-4-pentyl cyclohexyl) benzoate and 4-pentyl cyclohexyl-4-(4-propyl cyclohexyl) benzoate from optical studies, Mol. Cryst. Liq. Cryst. 409 (2004) 437–447.
[26] R.L. Danley, New heat flux DSC measurement technique, Thermochim. Acta 395 (2003) 201–208.
[27] K.-H. Illers, Die Ermittlung des Schmelzpunktes von kristallinen Polymeren mittels Wärmeflußkalorimetrie (DSC), Eur. Polym. J. 10 (1974) 911–916.
[28] Merck KGaA, Frankfurter Str. 250, D-64271 Darmstadt, Germany (EMD Chemicals, Inc. for North America). Catalog#: M-24: 100008.9005, HP-53: 100007.9005, BCH-52: 100006.9005.
[29] A. Hensel, C. Schick, Temperature calibration of temperature-modulated differential scanning calorimeters, Thermochim. Acta 305 (1997) 229–237.
[30] C. Schick, U. Jonsson, T. Vassilev, A. Minakov, J. Schawe, R. Scherrenberg, D. Lörinczy, Applicability of 8OCB for temperature calibration of temperature modulated calorimeters, Thermochim. Acta 347 (2000) 53–61.
[31] M. Castro, J.A. Puertolas, Simple accurate ac calorimeter for liquid-crystals and solid samples, J. Therm. Anal. 41 (1994) 1245–1252.
[32] U.G. Jonsson, O. Andersson, A. Fransson, Investigations of the temperature gradients affecting the temperature scale of a 3ω-heat capacity spectrometer, Thermochim. Acta 347 (2000) 45–51.